EasyChair Preprint

№ 9655

Guided Image Filter Inspired Improved Single Image Dehazing Method

Muhammad Shan Saleem, Gulistan Raja and Junaid Mir

February 3, 2023

Guided image filter inspired improved single image dehazing method

Muhammad Shan Saleem[1], Gulistan Raja[2], Junaid Mir[3]
[1,2,3]Electronics Engineering Department, University of Engineering and Technology, Taxila, Pakistan
Corresponding author: Muhammad Shan Saleem (e-mail: shansaleem15@gmail.com).

***Abstract*—With the recent proliferation of industries, traffic and wildfires, the haze is becoming a common atmospheric phenomenon which has a critical impact on the computer-vision based acquisition systems. To address the image degradation due to the hazy weather, we propose an improved physical model-based single image dehazing method. The proposed dehazing process includes the calculation of the atmospheric light value, estimation of the transmission map and finally, the restoration of scene radiance from the hazed image. The main contribution of this work is to combine the recent advances in the atmospheric light value calculation techniques with the utilization of refined guided filter by employing a colour image as guidance for the estimation of an optimized transmission map. The detailed qualitative and quantitative analysis of our proposed method with current state-of-the-art techniques, reveal that dehazed images generated from our algorithm are of improved visual quality with sufficient image details.**

***Keywords*—Atmospheric light scattering model, haze, guided image filter, koschmeider's law, single image dehazing**

Fig. 1. Examples of images before (top row) and after dehazing (bottom row) by our method.

I. Introduction

Haze is a natural atmospheric phenomenon in which smoke, dust and other dry particulates accumulate in the air. As these suspended small particles of different sizes result in the scattering, reflection and refraction of the atmospheric light, the haze has a critical impact on the image acquisition systems. Images acquired in the hazy weather have considerably reduced visibility, dynamic range and contrast and, therefore, may result in the loss of details. These factors can significantly impact the human visual system and computer vision systems recognition and matching capabilities due to difficulty in the identification of crucial object features. Figure 1 illustrates the examples of hazed and the corresponding dehazed images. The hazy images, as shown in Figure 1 (top row), are of low visual quality with reduced contrast and changed colours. Whereas, the dehazed images by our method, as shown in the bottom row of Figure 1, are of high contrast along with richer details and better visibility. Therefore, with haze becoming a common atmospheric phenomenon due to the recent proliferation of industries, traffic and wildfires, image dehazing techniques can play a pivotal role in areas such as astronomy, meteorology, traffic surveillance and computer vision [1]–[4].

Considering the importance of image dehazing techniques as mentioned above, a considerable amount of work has been carried out in this area over recent decades. The initial image dehazing methods were based on the conventional image enhancement techniques such as gamma transformations, histogram equalization, homomorphic filters, curvelet transforms, and the Retinex method [5]–[8]. Due to the inherent limitations like contrast and color distortion of the image enhancement techniques, the dehazing effect of these methods was rather limited. In this work, we present an effective single image-based dehazing technique by using the atmospheric light scattering physical model [7] which give more precise values of atmospheric light compared to previous studies. First, the atmospheric light value is estimated from the decision and dark channel images. The transmission map is then learned through an optimized guided image filter [28] due to its edge-preserving property and low computational cost. Finally, the dehazed image is obtained using the physical model. To the best of the authors' knowledge, no other technique has been reported with the collection of steps that have been employed in this work. In the end, a detailed evaluation of this proposed methodology is presented.

The remaining sections of the paper are arranged as follows: Section II first details the related image dehazing work. The relevant concepts involved in the image dehazing techniques are then described in Section III. Section IV presents the proposed methodology for image dehazing. Results and discussions are discussed in Section V. Finally, Section VI describes the conclusion and future work.

II. Related Work

Three different types of image dehazing techniques relying on physical light models have been proposed in the literature. The first type of physical model-based dehazing methods

uses multiple images captured in varying weather conditions or depth information. An atmospheric model-based binary scattering model is proposed by Narasimhan *et al.* [9], [11] and Nayar *et al.* [10]. It utilizes three-dimensional structural information determined from two or more climate images to reconstruct a true color dehazed image under unknown bad weather conditions. Method of Shwartz *et al.* [12] is based on the phenomena that light become partially polarized after scattering by atmospheric particles. Therefore, images acquired through a polarizer at different angles are utilized for image dehazing. However, this strategy cannot meet the requirements of a real physical model. These multiple images based methods mentioned above are not convenient for utilization in wide applications due to the need for multiple image acquisition and additional structural information.

The second type of physical model-based dehazing methods relies on a single image for dehazing and has gained significant achievements in recent years. Due to the single hazed image, less prior information is available for dehazed scene structure, making the image dehazing problem particularly challenging. Tan *et al.* [13] enhanced the hazed images by maximizing the local contrast. While this technique attains good results in natural scenes or thick fog, the dehazed image often has colour oversaturation with halos observed in depth variations in the scene. The statistics of haze-free outdoor images with soft matting interpolation technique are utilized by He *et al.* [14] to restore a dehazed image. While the method achieves good dehazing results, it has limitations when the object in the scene is inherently near to the airlight. Sulami *et al.* [15] addressed the problem of the automatic atmosphere optical vector calculation as this value plays a critical role in the performance evaluation of single image dehazing techniques. Yadav *et al.* [16] utilized adaptive gamma correction approach in order to minimize the colour distortion from hazed images. A guided filter is utilized by He *et al.* [17], [30] to reduce halo artifacts and refine a hazy image. A pixel-based dark channel referred to as a weak dark channel prior is presented in [18] for the transmission map and atmospheric light calculations. The atmospheric light value is calculated in the same manner as in the dark channel prior, but pixel-based guided filtering is used to refine the transmission map. In Tang *et al.* [19] method, guide images are designed to redress the bright region. This method gives good results in terms of image quality and detail as compared to classical methods. In the Salazar *et al.* method [20], the dark channel before modified in terms of computation resulted in fewer artifacts in restored images. This method is also suitable for real-time video processing. Airlight due to scattering, reflection and refraction changes the scene information and also has a negative impact on the dehazed image quality [21]. A multi-scale Retinex algorithm is proposed by Wang *et al.* [22], which is further improved to address the Retinex's lack of adaptation to the image scenario, which results in non-ideal dehazed image representation for heterogeneous haze in the scene [23]. Keeping in view all the discussion, it can be deduced that the physical model-based techniques for image dehazing have their limitations.

Third type of image dehazing techniques are based on deep learning. Many deep learning-based image dehazing methods have been proposed recently; however, most of these techniques ignore the atmospheric light estimation and fail to produce accurate transmission maps leading to inaccurate dehazing results [38]. An attenuation prior method is presented by Zhu *et al.* [24], which uses colour information based depth data attained through machine learning for building the transmission map. In Cai *et al.* [25] method, convolution neural network (CNN) based feature learning is performed for hazed images. However, an inaccurate outcome map may be obtained, leading to poor dehazing results in different specified hazed conditions. A coarse-grained transmission map estimation is performed using a coarse network in [26], which is further refined by fine networks. The shortcoming of this method is to adjust parameters manually for different hazed density in the image. The performance of dehazing techniques does not remain the same during different weather conditions as the fog in the atmosphere is non-homogeneous. The size of particles also varies, which badly affects the dehazing performance. Airlight due to scattering, reflection, and refraction changes the scene information and also has a negative impact on the dehazed image quality [27]. Therefore, there is an essential need to develop more robust image dehazing models that can retain full scene details and perform well in all weather and lighting conditions.

III. Preliminaries

Some basic concepts and methods which are used in this work are discussed in this section. First of all, the introduction to the atmospheric light scattering model is presented. Afterwards, we review the concepts of atmospheric light value calculation, which are followed by the description of a guided image filter in the end.

A. Atmospheric light scattering model

In image processing and computer vision, the visual attenuation model is defined by Koschmeider's law [29]. It elaborates the formation of a hazy image in a hazed environment and is given as

$$I(x) = J(x)t(x) + A(1 - t(x)), \tag{1}$$

where $I(x)$ is the captured input hazed image, $t(x)$ presents the transmission map of the scene, $J(x)$ is output dehazed image, A is the atmospheric light value. The transmission map keeps the information of a non-scattered portion of light. The objective is to extract the scene radiance $J(x)$ by estimating $t(x)$ and A from the hazed image $I(x)$. The product $t(x)J(x)$ in (1) is the direct attenuation whereas the subsequent product; $(1 - t(x))A$, is the airlight which is the light scattered by the particulates in the air. It can be observed that with reduced $t(x)$, the scene radiance diminishes and the airlight increases. Therefore, scene radiance is reduced due to the presence of haze and far objects and thereby, results in reduced image quality.

B. Atmospheric light value

The atmospheric light value A describes the surrounding light in the image. Generally, the value of A is calculated based on a hypothesis value [13]. The dark channel prior technique [14] uses the 0.100% of brightest pixels in the dark channel to calculate its numeric value. However, there will be an error in the estimation of A in the presence of white areas (e.g., snow) in the hazy image. In Tarel *et al.'s* method [23], the white balance of the hazed image is taken and white atmospheric optical value is utilized for dehazing. An automatic method for the computation of the atmospheric light value is presented in [15].

C. Guided image filter

The guided image filter is a smoothing operator that preserves the edges in the image considering the content of the guidance image [30], [31]. The guided image filter can also transfer the guidance image's structure to the filtering output. It is one of the fastest edge-preserving filter and non-approximate algorithms in computer graphics and computer vision. Along with filtering applications like guided feathering and dehazing, guided image filter has many applications in HDR image compression, detail enhancement, joint upsampling, edge-aware smoothing, and image matting.s For an input image p and the guidance image I, the output of the guided image filter q is represented through a local linear model:

$$q_i = b_k + a_k I_i, \quad \forall i \in w_k, \tag{2}$$

where b_k and a_k are the linear constant coefficients in a square window w_k having radius r which is centered at the pixel k. The cost function which is minimized in the guided filter for seeking the coefficient values (a_k, b_k) is given by

$$E(a_k, b_k) = \sum_{i \in w_k} ((a_k I_i + b_k - p_i)^2) + \epsilon a_k^2), \tag{3}$$

where ϵ is the regularizer having constant value 10^{-3}. After minimizing the above equation results in a least square problem with solution given by

$$a_k = \frac{\frac{1}{|w|}\sum_{i \in w_k} I_i p_i - \mu_k \bar{p_k}}{\sigma_k^2 + \epsilon} \text{ and } b_k = \bar{p_k} - a_k \mu_k, \tag{4}$$

where σ_k^2 is the variance and μ_k is the mean of I in the window w_k where $|w|$ is the number of pixels in the window. The final filtered output is given by

$$q_i = \frac{1}{|w|} \sum_{k | i \in w_k} (b_k + a_k I_i). \tag{5}$$

In the image dehazing work, the transmission map of the input image is usually estimated from the dark channel prior, which results in the significant loss of details and information in some areas of the image [14]. To overcome these issues, we have used the application of a guided image filter for dehazing purposes. Here transmission map is estimated from the hazy input image using a guided image filter.

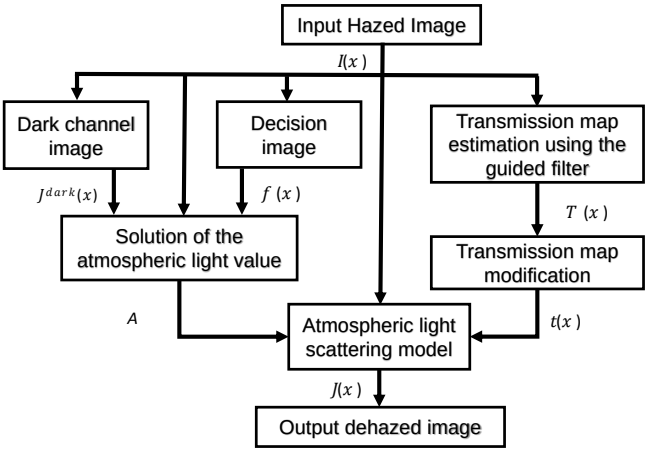

Fig. 2. Block diagram of the proposed single image dehazing method.

IV. Proposed Methodology

The proposed methodology for a single image dehazing algorithm comprises several steps which involve the calculation of the atmospheric light value, acquisition of the transmission map and the utilization of the atmospheric light scattering model. Figure 2 depicts the block diagram of our proposed method and the details of the processing steps are presented below.

A. Atmospheric light value

To compute the atmospheric light value A, we have opted for the technique proposed in [22], which is less complex, adaptive and content dependent in comparison to the previously proposed methods [14], [15], [23] for the atmospheric light value calculation. It is a three-step solution involving the computation of decision image $f(x)$, dark channel image $J_{\mathrm{d}}(x)$ and the calculation of atmospheric light value A.

1) Decision image: Represented by $f(x)$, decision image is computed as

$$f(x) = \sqrt{(r^2 + g^2 + b^2) - (r + g + b)^2/3)}, \tag{6}$$

where $\{r, g, b\}$ are the values of red, green and blue pixels in the colour channel. After setting a decision criterion threshold Δ which is defined as, if $f(x) \leq \Delta$, the pixel value is treated as bright inside the white section and is, therefore, discarded. Only the pixel values for which $f(x) > \Delta$, are used for the correct measurement of the atmospheric light illumination. The computed decision image $f(x)$ through (6) can be observed in the third column of Figure 3.

2) Dark channel image: $J_{\mathrm{dark}}(x)$ represents the dark channel image and is computed as [14], [32]

$$J_{\mathrm{dark}}(x) = \min_{c \in \{r,g,b\}} (\min_{y \in \Omega(x)} (I^c(y))), \tag{7}$$

where I^c is a single channel of colour image $I(x)$ in which $c \in \{r, g, b\}$, $\Omega(x)$ is x centered pixel's square patch. $J_{\mathrm{dark}}(x)$ is given by the product of two min operators; $\min_{c \in \{r,g,b\}}$

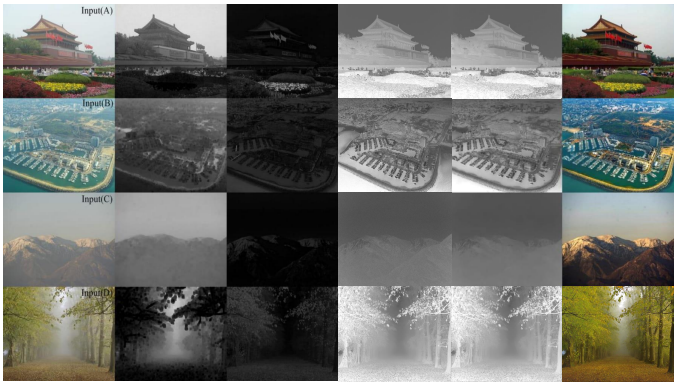

Fig. 3. The first column from the left showing different real input hazed images, i.e., A, B, C, and D. Second column showing dark channel images; the third column showing decision images; the fourth column is a rough transmission map obtained from guided image filter; the fifth column is optimized transmission map, and the sixth column is output dehazed images for A, B, C, and D, respectively.

Fig. 4. Results are obtained for different values of Δ. The first column is input images, and the second to fifth columns are output dehazed images for Δ=1, 2, 3, 4, respectively.

applied on every pixel in given RGB channel plane and $\min_{y\in\Omega(x)}$ is the minimum filter having patch size of 15×15 . Third column of Figure 3 shows the dark channel images $J_{\text{dark}}(x)$ computed through (7) for different input images.

3) Atmospheric light value solution: Dark channel image $J_{\text{d}}(x)$ and the decision image $f(x)$ are utilized for the computation of the atmospheric light value. For this, the brightest 0.100% pixels of the $J_{\text{d}}(x)$ are initially picked. Then, among these pixels, the ones with having corresponding $f(x)$ value higher than the threshold Δ are chosen. In the end, the atmospheric light value A is calculated by averaging of these chosen pixels. Figure 4 shows the results for different values of Δ. The threshold value of $\Delta = 2$ was utilized in the proposed algorithm, which was deemed sufficient for the efficient image dehazing results compared to other results.

B. Transmission map

The transmission map $t(x)$ is an alpha mapping which is a type of visible surface encompassing edges boundaries and depth of the scene objects for the estimation of the haze

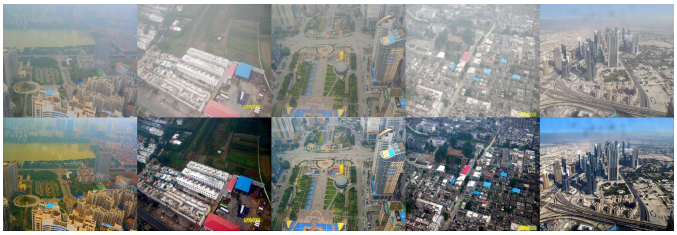

Fig. 5. Dehazing results of the aerial cityscape images. The top and bottom rows depict input hazed and corresponding output dehazed images, respectively.

Fig. 6. Dehazing results of the sky and thick fog images. The first and third column shows input hazed images. The corresponding dehazed images are presented in the second and the fourth column.

concentration. We have employed a guided image filter for the estimation of the transmission map because of its good colour constancy, dynamic range and colour balancing results in the output dehazed colour image. However, a rough transmission map $T(x)$ is obtained from guided image filter is shown in fourth column of Figure 3. Accuracy of the transmission map is further increased by the max filter of size 5×5 followed by the mean filter of size 3×3 in order to get the final optimized transmission map $t(x)$ shown in fifth column of Figure 3.

C. Restoration of scene radiance in the hazy image

Dehazed image is acquired from the atmospheric light scattering model by rewriting (1) as

$$J(x) = \frac{I(x) - A}{\max(t_0, t(x))}. \tag{8}$$

We have set t_0 to 0.05 for the optimized transmission map to avoid the random noise which can arise in the images. For example, the sky region of the first image in Figure 3 is partially white in the hazy (first image of the first row) and the dehazed representation (last image of the first row). Therefore, the shade of the sky will be closer to the computed atmospheric light value A. Hence, when the transmission map $t(x)$ of the sky region is nearly zero, the dehazed image will include random noise. The final dehazed images $J(x)$ are shown in the last column of Figure 3.

Fig. 7. Dehazing results of the real-world hazy images from the RESIDE dataset [35]. The top and bottom rows depict input hazed and corresponding output dehazed images, respectively.

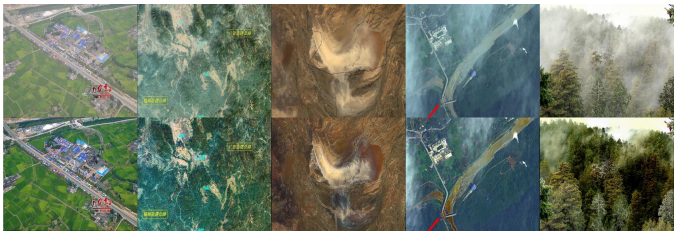

Fig. 8. Dehazing results of remote surveillance and forest images. The top and bottom rows depict input hazed and corresponding output dehazed images, respectively.

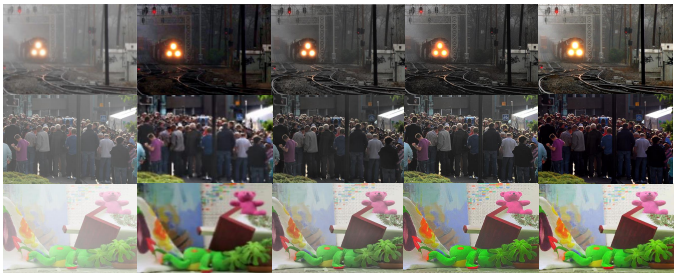

Fig. 9. Qualitative comparison of the hazy images. Most left column shows input hazy scenes and most right column is output results from our method. While second to fourth column show results obtained from, Haouassi *et al.* [38], Galdran *et al.* [36] and Dat *et al.* [37] method, respectively.

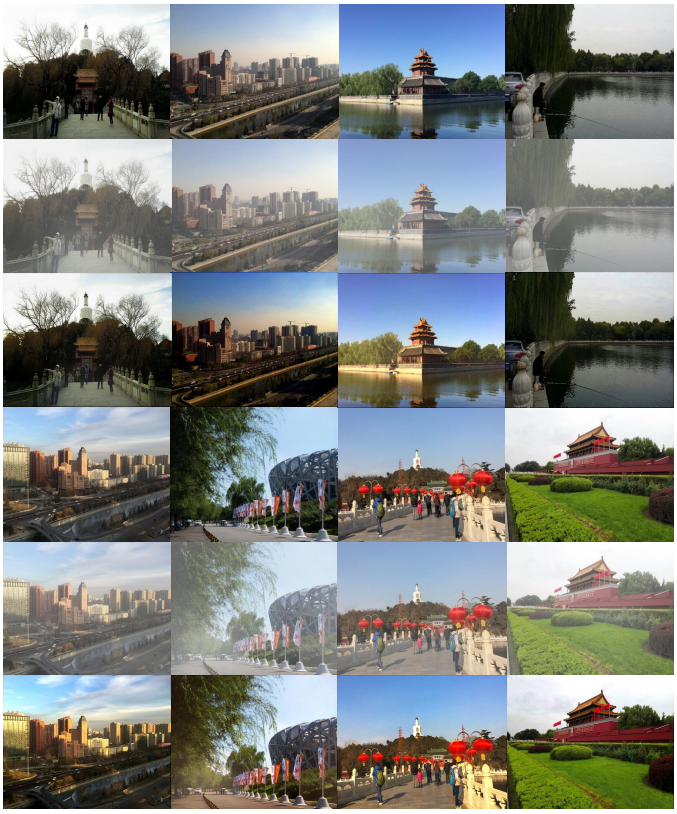

Fig. 10. Dehazing results of the synthetic images from the RESIDE dataset [35]. The first and fourth row shows the ground truth images, and the second and fifth row depicts hazed images. The third and sixth row presents dehazed output images from our proposed method, respectively.

V. Results and Discussions

The proposed dehazing algorithm is coded in MATLAB on the Windows OS desktop Intel Core i5 CPU@2.80 GHz processor. The evaluated images were taken from the standard datasets employed in the previous image dehazing works [13]–[15], [22], [33], RESIDE dataset [35] and from the public image library of the internet. Qualitative analysis of our algorithm with the recent state-of-the-art single image dehazing methods is presented in this section. Then, to contrast and compare the performance objectively, the quantitative analysis is presented along with the details of evaluation metrics employed for the performance comparison.

A. Qualitative analysis

For qualitative comparison and analysis of our proposed single image dehazing algorithm, the dehazed images are categorized into three classes based on the scene information. These classes include dehazed images of (i) aerial cityscapes, (ii) large sky area or dense fog, and (iii) forest images or remote surveillance.

Figure 5 shows the dehazing results from our proposed algorithm for flying cityscape images. These images generally have green spaces, structures and earth in the background with nearly no sky region. It can be observed that the dehazed images have an aesthetic effect, a noticeable structure restoration, extraordinary scene information, and fine colours with high brightness and contrast. Figure 6 and Figure 7 depicts the dehazing results for the images having a large sky area or thick fog. The dehazed images have a high picture differentiation contrast, an appropriate white balancing in the gray scene objects and clear structures with fine details. Further, gray sky areas in images; Road and Tiananmen, are also dehazed effectively by this proposed algorithm. In these images, the original gray sky is restored directly to a white sky as blue sky areas cannot be recovered by only using the physical models. This is due to the consistent gray level values in the sky area which results in RGB channel difference close to zero due to the zero value of $f(x)$. Figure 8 demonstrates the haze removing results from the forest and remote surveillance images. The impact is evident for the remote surveillance images. Although the first three images are effectively dehazed, fog and clouds are observed in the last

Fig. 11. Qualitative comparison of our proposed dehazing algorithm with other methods. The first column presents input hazed images A and B from left; the second, third and fourth column shows the dehazed images by He's [14], Wang's [22] and our proposed method.

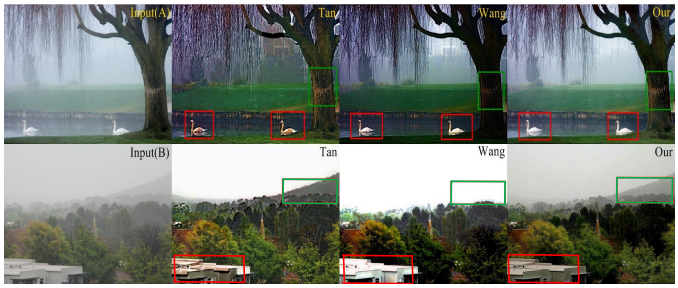

Fig. 12. Qualitative comparison of our proposed dehazing algorithm with other methods. The first column presents input hazed images A and B from left; the second, third and fourth column shows the dehazed images by Tan's [13], Wang's [22] and our proposed method.

Fig. 13. Qualitative comparison of our proposed dehazing algorithm with different latest methods. Left to right; input hazed images A and B; correspondingly output dehazed images by Kopf's [8], He's [14], Zhu's [24], Wang's [22], Fattal's [33], Nishino's [34] and our proposed method.

Fig. 14. Qualitative comparison of our proposed dehazing algorithm with different latest methods. Left to right; input hazed images A and B; correspondingly output dehazed images by Kopf's [8], He's [14], Zhu's [24], Wang's [22], Tarel's [23], Fattal's [33] and our proposed method.

two images. It can be seen that dehazing is more significant in the fog regions in comparison to the thick mist regions. In Figure 9, qualitative comparison of real world images is made between Haouassi *et al.* [38], Galdran *et al.* [36], Dat *et al.* [37] and our method, respectively. Better dehazing results are obtained by our method in all three images of Figure 9. In Figure 10, synthetic images are used from RESIDE dataset [35]. Resulted images obtained from our method are more close to ground truth images as shown. Based on the given results, we can infer that our proposed algorithm can be utilized for effective dehazing.

We have compared our work with the latest state-of-the-art single image dehazing methods [8], [13], [14], [22]–[24], [33], [34]. Among these methods, the techniques proposed by the Tan's [13], He's [14] and Wang's [22] are the most established and accepted ones. Figure 11 shows the dehazed images from the He's, Wang's and our proposed methods. In comparison, it can be seen that the image tone of the dehazed images from Wang *et al.'s* technique is better in comparison to the He *et al.'s* and our proposed method. However, colour cast can be observed in the blue box for input image B. Further, for input image A, the overall slightly red tone of the image is not preserved in the dehazed representation of the Wang's method. These shortcomings are not present in the He's and our method. In addition, our method is better in preserving the structure detail information in comparison to the He's technique as depicted in the green box for both input images A and B.

In Figure 12, we compare our dehazed images with Wang's and Tan's methods. While the dehazed images from both methods have improved visibility and image details, colours are oversaturated in the red boxes for both output images. Although the oversaturation is less in Wang's method, it cannot restore effectively the mountain part and pattern on the wood bark, as shown in the green boxes. In comparison, our method does not show any colour cast phenomena and the dehazed images are clear with details recovered. Finally, in Figures 13 and 14, we present the dehazed images from different single image dehazing methods. It can be observed that all of these techniques generally produce good dehazing results. However, some of these methods are superior in removing haze, avoiding oversaturation and colour cast, and in retaining details in comparison to the others. These differences can be better quantified through quantitative analysis by using objective metrics as the qualitative analysis can also be influenced by the viewer's artistic choice.

B. Quantitative analysis

In this section, evaluation metrics are first introduced and then the analysis of the objective dehazing results is presented.

1) Evaluation metrics: We tested three objective quality metrics for the quantitative performance comparison and analysis of the proposed image dehazing algorithm. These metrics were applied to the gray-scale conversions of the colour dehazed images.

Information entropy (IE) indicates the amount of randomness present in an image and its value quantifies image

information. IE in [22] is defined as

$$\text{IE} = -\sum_{i=0}^{N} P(x_i)\log_2(P(x_i)), \tag{9}$$

where n is the image bit depth and its value is 8, $N = 2^n - 1$ and $P(x_i)$ is the probability of image gray values obtained from the gray-scale histogram. IE value is maximum for the non-uniform images as the probability of all gray-values is the same. However, for hazy and gray-scale consistent images, the IE value is very low.

TABLE I
IMAGES EVALUATION METRIC OUTCOMES OF THE HE'S [14], WANG'S [22] AND OUR PROPOSED METHOD FOR FIGURE 11.

No.	Indicators	Input	He	Wang	Proposed
Input(A)	IE	6.4075	7.5790	**7.6233**	7.3095
	AG	0.0077	0.0211	0.0271	**0.0329**
	RMSE	—	63.920	73.058	**79.157**
Input(B)	IE	7.2301	7.6169	7.2041	**7.6690**
	AG	0.0225	0.0382	**0.0728**	0.0561
	RMSE	—	59.972	85.575	**87.274**

TABLE II
IMAGES EVALUATION METRIC RESULTS OF THE TAN'S [13], WANG'S [22] AND OUR PROPOSED METHOD FOR FIGURE 12.

No.	Indicators	Input	Tan	Wang	Proposed
Input(A)	IE	7.4738	7.1784	7.4325	**7.6599**
	AG	0.0158	0.0380	0.0353	**0.0395**
	RMSE	—	**81.715**	78.139	54.978
Input(B)	IE	6.7363	5.9215	4.8847	**7.0034**
	AG	0.0112	**0.0294**	0.0264	0.0153
	RMSE	—	49.664	55.089	**57.369**

Average gradient (AG) can detect the variations in detail for an image and describe its clearness. For a hazy image, AG in [22] is characterized as

$$\text{AG} = \frac{1}{M.N}\sum_{x=1}^{M}\sum_{y=1}^{N}\sqrt{\left(\frac{\delta I(x,y)}{\delta x}\right)^2 + \left(\frac{\delta I(x,y)}{\delta y}\right)^2}/2, \tag{10}$$

where M is the width and N is the height of the picture and $1 \le x \le M$, $1 \le y \le N$. For retaining better image details in the output dehazed image, value AG should be higher.

Root mean square error (RMSE) represents the precision between the contrast images that evaluates the amount of the image's data variation and is defined as

$$\text{RMSE} = \sqrt{\frac{1}{MN}\sum_{x=1}^{M}\sum_{y=1}^{N}(I(x,y) - J(x,y))^2}, \tag{11}$$

where $J(x,y)$ is the output dehazed image and $I(x,y)$ is the corresponding reference hazy image. The value of RMSE should be higher for good image quality and dehazing results in some extent [22], [39].

2) Objective results: For comparative quantitative analysis of the proposed dehazing algorithm with other methods, we have tabulated the evaluation metrics in Tables I, II, III, and IV. The objective is to achieve a high value of AG, IE and RMSE which is an indication of a clear, haze-free, accurate and detailed dehazed image representation. The highest quality in these tables is indicated in bold numbers.

In Table I, we have compared our proposed method with He *et al.'s* [14] and Wang *et al.'s* [22] methods. The high value of AG and RMSE for our proposed method indicates that this methodology can restore more details and retain high contrast in the dehazed images. The same can be inferred from the Table II, which presents the comparison with the Tan *et al.'s* [13] and Wang *et al.'s* [22] techniques. Finally, Table III and IV tabulates the evaluation metric results of different single image dehazing algorithms. Based on the three evaluation parameter values, which in most cases are the highest for our method, it can be established that our proposed single image dehazing method works well in comparison to the other techniques.

VI. CONCLUSION

In this paper, we have implemented a single image dehazing algorithm dependent on the physical atmospheric light scattering model and luminance components of an image, utilizing the guided image filter for the transmission map calculation. The effectiveness of this algorithm has been measured subjectively as well as objectively in terms of three evaluation parameters: IE, AG, and RMSE. The results obtained from our method demonstrate that it can successfully improve the nature of hazed images and synthetic images as well. However, there are few shortcomings when the hazed image has greenery along with the sky area but this method gives comparable results. While there are several approaches based on deep learning, the proposed method does not require a large number of training data and enables efficient processing which is suitable for embedded and mobile applications and systems.

REFERENCES

[1] Y. Lu and D. Song, "Visual navigation using heterogeneous landmarks and unsupervised geometric constraints," *IEEE Transactions on Robotics*, vol. 31, no. 3, pp. 736–749, 2015.

[2] F. Xie, M. Shi, Z. Shi, J. Yin, and D. Zhao, "Multilevel cloud detection in remote sensing images based on deep learning," *IEEE Journal of Selected Topics in Applied Earth Observations and Remote Sensing*, vol. 10, no. 8, pp. 3631–3640, 2017.

[3] S. Coşar, G. Donatiello, V. Bogorny, C. Garate, L. O. Alvares, and F. Brémond, "Toward abnormal trajectory and event detection in video surveillance," *IEEE Transactions on Circuits and Systems for Video Technology*, vol. 27, no. 3, pp. 683–695, 2016.

[4] U. Rosolia, S. De Bruyne, and A. G. Alleyne, "Autonomous vehicle control: A nonconvex approach for obstacle avoidance," *IEEE Transactions on Control Systems Technology*, vol. 25, no. 2, pp. 469–484, 2016.

[5] J. A. Stark, "Adaptive image contrast enhancement using generalizations of histogram equalization," *IEEE Transactions on image processing*, vol. 9, no. 5, pp. 889–896, 2000.

[6] E. H. Land, "Recent advances in retinex theory," *Central and peripheral mechanisms of colour vision*, pp. 5–17, 1985.

[7] Y. Gao, H.-M. Hu, S. Wang, and B. Li, "A fast image dehazing algorithm based on negative correction," *Signal Processing*, vol. 103, pp. 380–398, 2014.

TABLE III
IMAGES EVALUATION METRIC RESULTS OF THE KOPF'S [8], HE'S [14], ZHU'S [24], WANG'S [22], FATTAL'S [33], NISHINO'S [34] AND OUR PROPOSED METHOD FOR FIGURE 13.

No.	Indicators	Input	Kopf	He	Zhu	Wang	Fattal	Nishino	Proposed
Input(A)	IE	7.5064	7.6319	7.4461	7.5191	7.3530	7.7547	7.2515	**7.5854**
	AG	0.0159	0.0230	0.0196	0.0169	0.0244	0.0248	0.0259	**0.0277**
	RMSE	——	30.5710	25.5850	60.8510	66.9350	41.1590	66.0180	**69.8920**
Input(B)	IE	7.3562	7.5858	7.5399	7.0498	7.6943	7.6494	7.4920	**7.7018**
	AG	0.0244	0.0296	0.0276	0.0251	0.0313	0.0321	0.0367	**0.0428**
	RMSE	——	22.6740	19.4620	**69.3670**	25.8400	24.5380	53.3380	38.2150

TABLE IV
IMAGES EVALUATION METRIC RESULTS OF THE KOPF'S [8], HE'S [14], ZHU'S [24], WANG'S [22], TAREL'S [23], FATTAL'S [33] AND OUR PROPOSED METHOD FOR FIGURE 14.

No.	Indicators	Input	Kopf	He	Zhu	Wang	Tarel	Fattal	Proposed
Input(A)	IE	7.4098	7.7923	7.8190	7.1196	7.8069	7.4590	**7.9087**	7.7928
	AG	0.0231	0.0341	0.0343	0.0243	0.0340	0.0331	0.0372	**0.0498**
	RMSE	——	32.2600	32.5520	**79.0050**	22.4560	54.0320	41.4680	38.9326
Input(B)	IE	7.7192	7.2360	6.9930	6.8310	7.1631	7.3465	6.9566	**7.3623**
	AG	0.0240	0.0311	0.0330	0.0237	0.0445	0.0377	0.0412	**0.0451**
	RMSE	——	28.8060	46.0950	**64.5040**	37.9510	34.4930	51.2640	53.2719

[8] J. Kopf, B. Neubert, B. Chen, M. Cohen, D. Cohen-Or, O. Deussen, M. Uyttendaele, and D. Lischinski, "Deep photo: Model-based photograph enhancement and viewing," *ACM transactions on graphics (TOG)*, vol. 27, no. 5, pp. 1–10, 2008.

[9] S. G. Narasimhan and S. K. Nayar, "Chromatic framework for vision in bad weather," in *Proceedings IEEE Conference on Computer Vision and Pattern Recognition. CVPR 2000 (Cat. No. PR00662)*, vol. 1. IEEE, 2000, pp. 598–605.

[10] S. K. Nayar and S. G. Narasimhan, "Vision in bad weather," in *Proceedings of the Seventh IEEE International Conference on Computer Vision*, vol. 2. IEEE, 1999, pp. 820–827.

[11] S. G. Narasimhan and S. K. Nayar, "Interactive (de) weathering of an image using physical models," in *IEEE Workshop on color and photometric Methods in computer Vision*, vol. 6, no. 6.4. France, 2003, p. 1.

[12] S. Shwartz, E. Namer, and Y. Y. Schechner, "Blind haze separation," in *2006 IEEE Computer Society Conference on Computer Vision and Pattern Recognition (CVPR'06)*, vol. 2. IEEE, 2006, pp. 1984–1991.

[13] R. T. Tan, "Visibility in bad weather from a single image," in *2008 IEEE Conference on Computer Vision and Pattern Recognition*. IEEE, 2008, pp. 1–8.

[14] K. He, J. Sun, and X. Tang, "Single image haze removal using dark channel prior," *IEEE transactions on pattern analysis and machine intelligence*, vol. 33, no. 12, pp. 2341–2353, 2010.

[15] M. Sulami, I. Glatzer, R. Fattal, and M. Werman, "Automatic recovery of the atmospheric light in hazy images," in *2014 IEEE International Conference on Computational Photography (ICCP)*. IEEE, 2014, pp. 1–11.

[16] S. K. Yadav and K. Sarawadekar, "Single image dehazing using adaptive gamma correction method," in *TENCON 2019-2019 IEEE Region 10 Conference (TENCON)*. IEEE, 2019, pp. 1752–1757.

[17] K. He, J. Sun, and X. Tang, "Guided image filtering," *IEEE transactions on pattern analysis and machine intelligence*, vol. 35, no. 6, pp. 1397–1409, 2012.

[18] C.-H. Hsieh, Q. Zhao, and W.-C. Cheng, "Single image haze removal using weak dark channel prior," in *2018 9th International Conference on Awareness Science and Technology (iCAST)*. IEEE, 2018, pp. 214–219.

[19] L. Tang, "Image haze removal using dark channel prior based on guided image," in *IOP Conference Series: Materials Science and Engineering*, vol. 787, no. 1. IOP Publishing, 2020, p. 012006.

[20] S. Salazar-Colores, J.-M. Ramos-Arreguín, J.-C. Pedraza-Ortega, and J. Rodríguez-Reséndiz, "Efficient single image dehazing by modifying the dark channel prior," *EURASIP Journal on Image and Video Processing*, vol. 2019, no. 1, pp. 1–8, 2019.

[21] J. Mai, Q. Zhu, and D. Wu, "The latest challenges and opportunities in the current single image dehazing algorithms," in *2014 IEEE international conference on robotics and biomimetics (ROBIO 2014)*. IEEE, 2014, pp. 118–123.

[22] J. Wang, K. Lu, J. Xue, N. He, and L. Shao, "Single image dehazing based on the physical model and msrcr algorithm," *IEEE Transactions on Circuits and Systems for Video Technology*, vol. 28, no. 9, pp. 2190–2199, 2017.

[23] J.-P. Tarel, N. Hautiere, A. Cord, D. Gruyer, and H. Halmaoui, "Improved visibility of road scene images under heterogeneous fog," in *2010 IEEE Intelligent Vehicles Symposium*. IEEE, 2010, pp. 478–485.

[24] Q. Zhu, J. Mai, and L. Shao, "A fast single image haze removal algorithm using color attenuation prior," *IEEE transactions on image processing*, vol. 24, no. 11, pp. 3522–3533, 2015.

[25] B. Cai, X. Xu, K. Jia, C. Qing, and D. Tao, "Dehazenet: An end-to-end system for single image haze removal," *IEEE Transactions on Image Processing*, vol. 25, no. 11, pp. 5187–5198, 2016.

[26] W. Ren, S. Liu, H. Zhang, J. Pan, X. Cao, and M.-H. Yang, "Single image dehazing via multi-scale convolutional neural networks," in *European conference on computer vision*. Springer, 2016, pp. 154–169.

[27] W. Wang, F. Chang, T. Ji, and X. Wu, "A fast single-image dehazing method based on a physical model and gray projection," *IEEE Access*, vol. 6, pp. 5641–5653, 2018.

[28] J. Pang, O. C. Au, and Z. Guo, "Improved single image dehazing using guided filter," in *Proc. APSIPA ASC*, 2011, pp. 1–4.

[29] H. Koschmieder, "Theorie der horizontalen sichtweite," *Beitrage zur Physik der freien Atmosphare*, pp. 33–53, 1924.

[30] K. He, J. Sun, and X. Tang, "Guided image filtering," *IEEE transactions on pattern analysis and machine intelligence*, vol. 35, no. 6, pp. 1397–1409, 2012.

[31] He, Kaiming and Sun, Jian and Tang, Xiaoou, "Guided image filtering," in *European conference on computer vision*. Springer, 2010, pp. 1–14.

[32] J.-B. Wang, N. He, L.-L. Zhang, and K. Lu, "Single image dehazing with a physical model and dark channel prior," *Neurocomputing*, vol. 149, pp. 718–728, 2015.

[33] R. Fattal, "Single image dehazing," *ACM transactions on graphics (TOG)*, vol. 27, no. 3, pp. 1–9, 2008.

[34] K. Nishino, L. Kratz, and S. Lombardi, "Bayesian defogging," *International journal of computer vision*, vol. 98, no. 3, pp. 263–278, 2012.

[35] B. Li, W. Ren, D. Fu, D. Tao, D. Feng, W. Zeng, and Z. Wang, "Benchmarking single-image dehazing and beyond," *IEEE Transactions on Image Processing*, vol. 28, no. 1, pp. 492–505, 2018.

[36] A. Galdran, "Image dehazing by artificial multiple-exposure image fusion," *Signal Processing*, vol. 149, pp. 135–147, 2018.

[37] D. Ngo, S. Lee, Q.-H. Nguyen, T. M. Ngo, G.-D. Lee, and B. Kang, "Single image haze removal from image enhancement perspective for real-time vision-based systems," *Sensors*, vol. 20, no. 18, p. 5170, 2020.

[38] S. Haouassi and D. Wu, "Image dehazing based on (cmtnet) cascaded multi-scale convolutional neural networks and efficient light estimation algorithm," *Applied Sciences*, vol. 10, no. 3, p. 1190, 2020.
[39] Z. Wang, A. C. Bovik, H. R. Sheikh, and E. P. Simoncelli, "Image quality assessment: from error visibility to structural similarity," *IEEE transactions on image processing*, vol. 13, no. 4, pp. 600–612, 2004.
[40] X. Qin, Z. Wang, Y. Bai, X. Xie, H. Jia, "FFA-net: Feature fusion attention network for single image dehazing," *Proc. AAAI Conf. Artif. Intell.*, vol. 34, no. 7, pp. 11908–11915, 2020.